Upper bound analysis of differential velocity sideways extrusion process for curved profiles using a fan-shaped flow line model

Zhou, Wenbin; Shi, Zhusheng; Lin, Jianguo

DOI:
10.1016/j.ijlmm.2018.03.004

Publication date:
2018

International Journal of Lightweight Materials and Manufacture 1 (2018) 21–32

Contents lists available at ScienceDirect

International Journal of Lightweight Materials and Manufacture

journal homepage: https://www.sciencedirect.com/journal/international-journal-of-lightweight-materials-and-manufacture

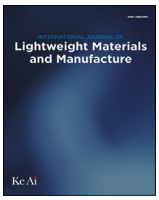

Original Article

Upper bound analysis of differential velocity sideways extrusion process for curved profiles using a fan-shaped flow line model

Wenbin Zhou, Zhusheng Shi*, Jianguo Lin

Department of Mechanical Engineering, Imperial College London, London SW7 2AZ, UK

ARTICLE INFO

Article history:
Received 30 January 2018
Received in revised form
16 March 2018
Accepted 16 March 2018
Available online 26 March 2018

Keywords:
Section profiles
Bending
Curvature
Extrusion
Upper bound method
Continuous flow line function

ABSTRACT

An analytical model for predicting the shapes of rectangular bars with variable curvatures along their lengths through a novel forming method, differential velocity sideways extrusion (DVSE), previously proposed by the authors, has been developed on the basis of the upper bound method. A new flow line function was presented to describe its deformation field. The plastic deformation zone (PDZ) was assumed to be fan-shaped, where the trajectory of the material flow within the PDZ had an elliptic shape. The proposed continuous flow line function was validated using finite element simulations. The flow patterns, extrusion pressure, curvature, and effective strain predicted by the analytical solutions agreed well with modelling results. Compared to the classical discontinuous simple shear model of channel angular extrusion (CAE) with a 90° die, the new approach was shown to predict the effective strain more closely.

1. Introduction

The demand for using extruded aluminium profiles as structural components on aircraft, trains and cars has been increasing nowadays due to lightweight design, where a reduced consumption of fuel and therefore a decreased emission of CO_2 can be achieved. In automobiles, aerospace, and shipbuilding industry, curved profiles are largely used for the manufacturing of ultra-light complex structures with high stiffness and strength due to aerodynamics, structural properties, and design reasons [1–4].

Curved profiles are mostly achieved by conventional bending procedures such as stretch bending, press bending, rotary draw bending and roll bending. However, most of them have disadvantages such as cross-section deformations and springback of profiles during the bending process which need to be avoided through expensive tools [5–10], thus inevitably significantly increasing the manufacturing costs. Some novel stress superposed cold bending techniques, i.e. torque superposed spatial (TSS) bending and superposed three-roll-bending with subsequent profile deflection, have been proposed to improve the forming limitations [11–14]. It was found that cross-sectional deformations and springback of curved profiles can be greatly reduced because of the superposition of torsion or compression with the external bending moment.

Recently, several novel extrusion-bending integrated methods have been developed. One is curved profile extrusion (CPE) proposed by Kleiner and co-workers [15,16] to decrease the manufacturing procedures of curved profiles. During CPE the metal billets are directly formed into curved profiles within only one extrusion procedure, thus significantly improving the manufacturing efficiency. This method is based on the conventional straight extrusion process, where a bending device is directly installed behind the die exit orifice to deflect the extruded profile so that it comes out of the die with the prescribed curvature. Muller [17,18] used a segmented regulating guiding device which is composed of serially placed bending discs at the die exit, to bend the extruded profile. Another way of extruding curved profiles is by exploiting an inclined die to adjust the material flow velocity distribution over the profile cross-section. Shiraishi and co-workers [19–21] developed a novel extrusion-bending integrated forming process for producing curved bars and tubes, in which a plasticine billet is extruded through a die aperture inclined towards the central axis of the container at a predetermined angle. It was found that the curvature of the extruded bars and tubes can be varied by adjusting the inclination angle of the die aperture, i.e., a greater inclination angle results in a greater curvature.

* Corresponding author.
E-mail address: zhusheng.shi@imperial.ac.uk (Z. Shi).

Peer review under responsibility of Editorial Board of International Journal of Lightweight Materials and Manufacture.

https://doi.org/10.1016/j.ijlmm.2018.03.004

Nomenclature

D_1	Width of the billet (mm)
D_2	Width of the extruded profile (mm)
dh, dl	Height and length of the differential element of the plastic deformation zone (PDZ) (mm)
dV	Volume of the differential element of the PDZ (mm^3)
h	Height of the dead metal zone (DMZ) (mm)
k_0, k_f	Initial and final shear yield stresses of the material (MPa)
$\overline{k}$	Mean shear yield stress of the material (MPa)
l	Die bearing length (mm)
l_1, l_2	Transient billet lengths with velocity v_1, v_2 respectively (mm)
m	Constant friction factor
P_1, P_2	Extrusion pressures of the upper and lower punches (MPa)
P_{1u}, P_{2u}	Upper bound of extrusion pressures of the upper and lower punches (MPa)
R_c	Bending radius of the profile (mm)
S_0	Cross-sectional area of the billet (mm^2)
S_3, S_4	Cross-sectional areas of the related profile (mm^2)
S_f, S_v	Areas of frictional and velocity discontinuity surfaces (mm^2)
Δv	Amount of velocity discontinuity (mm/s)
v_1, v_2	Extrusion velocities of the upper and lower punches (mm/s)
v_{1e}, v_{2e}	Maximum and minimum material flow velocities across the die exit orifice (mm/s)
v_3, v_4	Velocities at the volume (mass) centre of the related profile (mm/s)
v_p	Velocity of particle p moving on the curve MN (mm/s)
w	Thickness of the billet and extruded profile (mm)
$\dot{W}_{def}$	Power dissipated in the plastic deformation zone (N·mm/s)
$\dot{W}_e, \dot{W}_i$	External and internal power supplies (N·mm/s)
$\dot{W}_{S_f}, \dot{W}_{S_v}$	Power dissipated on the frictional and velocity discontinuity surfaces (N·mm/s)
$\overline{y}_3, \overline{y}_4$	Coordinates of the volume (mass) centre of the related profile (mm)

Greek symbols

θ	Angular position along the flow line (°)
$\overline{\varepsilon}$	Effective strain
$\dot{\overline{\varepsilon}}, \dot{\overline{\varepsilon}}_m$	Effective strain rate, mean value of the effective strain rate of the PDZ (s^{-1})
κ	Bending curvature of the extruded profile (mm^{-1})
λ	Extrusion ratio
ξ	Eccentricity ratio

The authors proposed a novel extrusion-bending process, named differential velocity sideways extrusion (DVSE), and its feasibility was studied [22,23]. The basic principle of this method is bending profiles simultaneously while extruding, which is achieved by controlling the gradient of the internal material flow velocity at the die exit orifice owing to the difference of relative moving velocities of two extrusion punches. It has been experimentally shown that by adjusting the extrusion velocity ratio of the two opposed punches as well as the extrusion ratio, curved profiles with adjustable curvatures can be obtained in one procedure. The quantitative relationship between curvature of the extrudate and the process parameters (the punch velocity ratio, extrusion ratio etc.) need to be developed for guiding the tooling design and forming process. Generally this can be achieved by theoretical analysis and numerical simulation such as the finite element (FE) modelling. The upper bound theorem has been extensively used to predict the forming pressure and analyse the deformation characteristics in the extrusion of profiles, ring rolling and forging processes, and to determine and minimise the exit profile curvature in the extrusion process of non-symmetrical profiles [24–28], etc. An approximate analytical model for predicting the forming pressure and curvature of the extrudate (round bar) has been developed by the authors based on the upper bound method and the rigid block model, where the plastic deformation zone (PDZ) was considered as consisting of several single shear planes and the modes of deformation were composed of rigid blocks of material separated by the velocity discontinuity planes [29]. The simple shear model is normally used in the upper bound analysis for approximation especially when the geometry is complex, e.g., 3D round bars in Ref [29]. In practice, material flow should be continuous without velocity discontinuity. On the other hand, FE modelling has also been widely used in the metal forming process since it can provide an accurate visual description of the material flow. However, one simulation case of the DVSE process requires huge computational resources. It is not efficient to design the DVSE process by FE modelling directly since numerous computations at different process conditions are needed. Instead, analytical expression can be achieved by upper bound theorem, which can be more easily applied in the process design and optimisation.

Therefore, in this paper, an upper-bound model, based on a more precise and realistic fan-shaped flow line model in which any part of the material will face a gradual and continuous change in its velocity rather than abrupt variations (velocity discontinuity) throughout the deformation process, is proposed for estimating the distribution of the dead metal zone (DMZ), extrusion pressure, curvature and effective strain of the extruded profile during the novel DVSE process. To focus on the flow field in the PDZ of the DVSE process, the geometry factor in the previous work [29] is simplified here by studying a rectangular bar, where the thicknesses of the die entrance and exit channels are the same in the configuration of the DVSE process. A finite element model has been developed in parallel with the analytical model to assess the accuracy and validity of the model. The effects of extrusion velocity ratio and extrusion ratio were investigated in detail. The new approach is also compared to the classical discontinuous simple shear model of channel angular extrusion (CAE) with a 90° die. The findings provide a deeper understanding needed for wider application of the DVSE forming technique.

2. Theoretical model

2.1. Upper bound model

The present analytical method is formulated on the basis of the upper bound theorem for a rectangular material undergoing plane strain extrusion, i.e. strain along thickness direction (normal to the paper) is assumed to be zero. This happens when the thicknesses of the die entrance and exit channels are the same in the configurations of the DVSE process. Similar assumption has been made previously by Kwan and co-workers [30], in which they argued that the process of equal-cross-section lateral extrusion may be assumed as a plane-strain problem, even if the cross-section is

circular, rectangular or any other shape. As shown in Fig. 1a, consider a T-shape die through which a plastic material is being pushed oppositely by pressures P_1 and P_2. The corresponding velocities of the two punches are v_1 and v_2, respectively. The initial widths of the billet and the container are both D_1, the final widths of the extruded profile and the die exit channel are both D_2. For a rigid-plastic material and amongst all the kinematically admissible velocity fields, the actual one minimises the power required for material deformation:

$$\dot{W}_i = 2\int_V \bar{k}\sqrt{\frac{1}{2}\dot{\varepsilon}_{ij}\dot{\varepsilon}_{ij}}dV + \int_{S_v} k\,\Delta v\,dS_v + \int_{S_f} mk\,\Delta v\,dS_f - \int_{S_t} P_i v_i dS \tag{1}$$

where k and $\bar{k}$ are the current and mean shear yield stresses of the material, $\dot{\varepsilon}_{ij}$ is the strain rate tensor, m is the constant friction factor, V is the volume of the plastic deformation zone (PDZ), S_v and S_f are the areas of velocity discontinuity and frictional surfaces respectively, S_t is the area where tension may occur, Δv is the amount of velocity discontinuity on the frictional and discontinuity surfaces, v_i and P_i are the velocity and traction applied on S_t, respectively.

Upper bound analyses normally involve assuming several velocity discontinuity surfaces, the material suddenly changes its velocity when it passes through them [31]. However, in reality the flow velocity does not experience abrupt variations after going through an infinitesimal surface. Here, an upper bound analysis is utilised where each point of the material will flow on a specific elliptical streamline and undergo gradual and continuous change in velocity. Fig. 1b shows the deformation model and a representative streamline $M'MNN'$ for the plane strain extrusion in which no strain exists normal to the paper. The volume considered for analysis is divided into five regions. Regions I ~ II are the PDZ in which the material undergoes plastic deformation. Region V is the dead metal zone (DMZ) whose central extension line BG divides the PDZ and the die exit channel into two parts, namely AB of length ξD_2 and CB of length $(1-\xi)D_2$. Here the variable $\xi = g(v_2/v_1, \lambda)$ represents the effect of v_2/v_1 on the PDZ and DMZ for a given extrusion ratio $\lambda = D_1/D_2$. The material flowing into these two parts comes from the corresponding two extrusion punches. The area of the DMZ and the position of the line BG vary with v_2/v_1 and λ. When $v_2/v_1 = 1$, line BG is exactly in the centre of the die exit channel. As v_2/v_1 decreases, it moves towards the side which has a lower extrusion velocity (v_2). The particle of the material on the inlet streamline $M'M$ will move along the curved line MN in region I where its velocity vector will undergo gradual and continuous variations in magnitude and orientation from $\vec{v_1}$ (rightward) at M to $\vec{v_3}$ (upward) at N. The key of upper bound analysis for this configuration of the DVSE process is to find such curves in region I (such as MN) tangent to the inlet and outlet streamlines (such as $M'M$, NN'). The solution is a quarter of an elliptical curve with its horizontal axial length 2b being $D_1/(\xi D_2) = \lambda/\xi$ times the vertical axial length $2a$. The streamline in region II has similar characteristics and can be obtained by respectively substituting ξ, v_1 with $1-\xi, v_2$. It should be noted that $v_3 = D_1 v_1/(\xi D_2) = \lambda v_1/\xi$ and $v_4 = \lambda v_2/(1-\xi)$ (from volume constancy) shown in Fig. 1b are the mean velocities at the centres of volume (mass) of the profiles coming out of regions III and IV, respectively, since there is no velocity discontinuity between regions III and IV, and the velocity for the material flowing out of the die exit should present a gradient where the upper side has the maximum velocity v_{1e}, the lower side has the minimum velocity v_{2e} and the boundary FG has the continuous velocity v_m. The die exit channel of the DVSE is sufficiently short to ensure the differential velocities are not compromised by the friction of the die bearing land [23].

The velocity vector of a particle moving on the elliptical curve MN is

$$\vec{v_P} = \frac{d\overrightarrow{EP}}{dt} = \frac{d\overrightarrow{EO'}}{dt} + \frac{d\overrightarrow{O'P}}{dt} = \frac{d\overrightarrow{O'P}}{dt} = \frac{d\vec{r}}{dt} \tag{2}$$

An elliptical curve having a horizontal axial length λ/ξ times the size of the vertical axial length is

$$\frac{x^2}{a^2} + \frac{y^2}{b^2} = 1 \tag{3}$$

where $b = (\lambda/\xi)a = m_1 a$, $x = -r\cos\theta$, $y = r\sin\theta$, then

$$r = \frac{m_1 a}{\sqrt{1 + (m_1^2 - 1)\cos^2\theta}} \tag{4}$$

Let $\vec{i}$, $\vec{j}$, $\vec{k}$ be the unit base vectors of the Cartesian coordinates, then

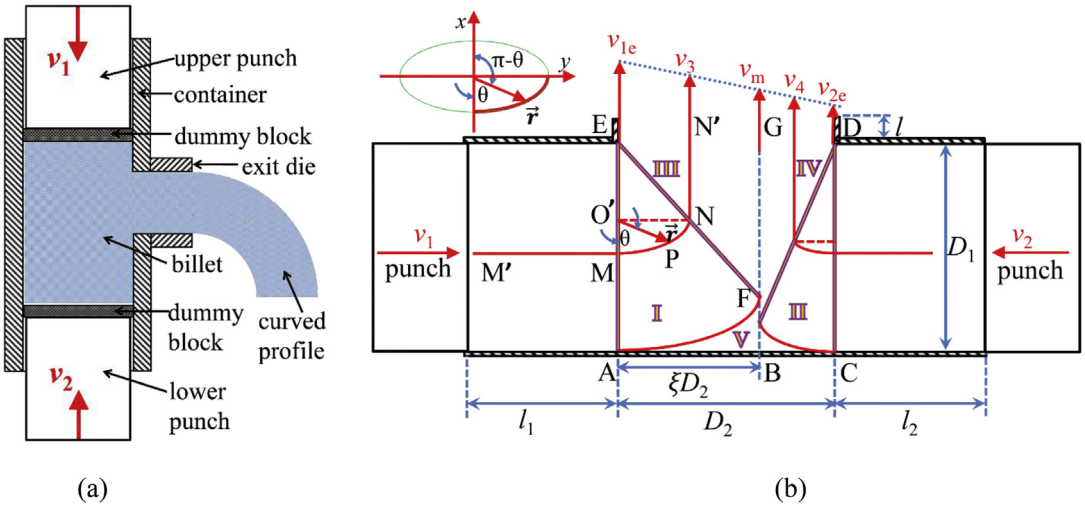

Fig. 1. (a) Schematic of the differential velocity sideways extrusion (DVSE) process [29], (b) the deformation model considered for analysis of the DVSE process.

$$\vec{r} = r\left(-\cos\theta\,\vec{i} + \sin\theta\,\vec{j}\right) = \frac{m_1 a}{\sqrt{1+(m_1^2-1)\cos^2\theta}}\left(-\cos\theta\,\vec{i} + \sin\theta\,\vec{j}\right) \tag{5}$$

Substituting Eq. (5) into Eq. (2), the velocity vector is expressed as

$$\vec{v_P} = \frac{a m_1 (m_1^2-1)\sin\theta\cos\theta}{\left[1+(m_1^2-1)\cos^2\theta\right]^{\frac{3}{2}}}\frac{d\theta}{dt}\left(-\cos\theta\,\vec{i} + \sin\theta\,\vec{j}\right) + \frac{m_1 a}{\sqrt{1+(m_1^2-1)\cos^2\theta}}\frac{d\theta}{dt}\left(\sin\theta\,\vec{i} + \cos\theta\,\vec{j}\right) + 0\,\vec{k} \tag{6}$$

Eq. (6) needs to satisfy the following boundary conditions:

$$\text{at entrance}: \ \vec{v_P} = v_1\,\vec{j}, \theta = 0 \Rightarrow a\frac{d\theta}{dt}\,\vec{j} = v_1\,\vec{j} \tag{7}$$

$$\text{at exit}: \ \vec{v_P} = m_1 v_1\,\vec{i}, \theta = \frac{\pi}{2} \Rightarrow m_1 a\frac{d\theta}{dt}\,\vec{i} = m_1 v_1\,\vec{i} \tag{8}$$

It can be seen from Eqs. (7)–(8) that the velocity field satisfies the geometry boundary conditions. For any streamline in the PDZ the angular velocity is a constant, which is $d\theta/dt = v_1/a$. Then the velocity field in the x–y–z reference system is

$$\vec{v_P} = \left[\,\vec{i} \quad \vec{j} \quad \vec{k}\,\right]\begin{bmatrix} -L\cos\theta + M\sin\theta \\ L\sin\theta + M\cos\theta \\ 0 \end{bmatrix}_{x,y,z} \tag{9}$$

where

$$L = \frac{m_1(m_1^2-1)\sin\theta\cos\theta}{\left[1+(m_1^2-1)\cos^2\theta\right]^{\frac{3}{2}}}\,v_1$$

$$M = \frac{m_1}{\sqrt{1+(m_1^2-1)\cos^2\theta}}\,v_1 \tag{10}$$

It is much more convenient to express the velocity field in cylindrical coordinates. Let $\vec{e_r}$, $\vec{e_\theta}$ be the unit base vectors of the polar coordinates and $\vec{e_z}$ the height unit vector, according to the coordinates system in Fig. 1b:

$$\left[\,\vec{i} \quad \vec{j} \quad \vec{k}\,\right] = \left[\,\vec{e_r} \quad \vec{e_\theta} \quad \vec{e_z}\,\right]T \tag{11}$$

where T is the transformation matrix

$$T = \begin{bmatrix} \cos(\pi-\theta) & \sin(\pi-\theta) & 0 \\ -\sin(\pi-\theta) & \cos(\pi-\theta) & 0 \\ 0 & 0 & -1 \end{bmatrix} \tag{12}$$

Substituting Eqs. (11) and (12) into Eq. (9), the velocity field in the r–θ–z reference system is

$$\vec{v_P} = \left[\,\vec{e_r} \quad \vec{e_\theta} \quad \vec{e_z}\,\right] \times \begin{bmatrix} \cos(\pi-\theta) & \sin(\pi-\theta) & 0 \\ -\sin(\pi-\theta) & \cos(\pi-\theta) & 0 \\ 0 & 0 & -1 \end{bmatrix}\begin{bmatrix} -L\cos\theta + M\sin\theta \\ L\sin\theta + M\cos\theta \\ 0 \end{bmatrix}_{r,\theta,z} = \left[\,\vec{e_r} \quad \vec{e_\theta} \quad \vec{e_z}\,\right]\begin{bmatrix} v_r \\ v_\theta \\ v_z \end{bmatrix}_{r,\theta,z} \tag{13}$$

The components of the velocity tensor would be

$$v_r = L = \frac{m_1(m_1^2-1)\sin\theta\cos\theta}{\left[1+(m_1^2-1)\cos^2\theta\right]^{\frac{3}{2}}}\,v_1$$

$$v_\theta = -M = \frac{-m_1}{\sqrt{1+(m_1^2-1)\cos^2\theta}}\,v_1$$

$$v_z = 0 \tag{14}$$

The components of the strain rate tensor can be obtained as

$$\dot{\varepsilon}_{rr} = \frac{\partial v_r}{\partial r} = 0$$

$$\dot{\varepsilon}_{zz} = \frac{\partial v_z}{\partial z} = 0$$

$$\dot{\varepsilon}_{\theta\theta} = \frac{v_r}{r} + \frac{1}{r}\frac{\partial v_\theta}{\partial\theta} = \frac{v_1}{r}\left\{\frac{m_1(m_1^2-1)\sin\theta\cos\theta}{\left[1+(m_1^2-1)\cos^2\theta\right]^{\frac{3}{2}}} - \frac{m_1(m_1^2-1)\sin\theta\cos\theta}{\left[1+(m_1^2-1)\cos^2\theta\right]^{\frac{3}{2}}}\right\} = 0$$

$$\dot{\varepsilon}_{rz} = \frac{1}{2}\left(\frac{\partial v_r}{\partial z} + \frac{\partial v_z}{\partial r}\right) = 0$$

$$\dot{\varepsilon}_{\theta z} = \frac{1}{2}\left(\frac{\partial v_\theta}{\partial z} + \frac{1}{r}\frac{\partial v_z}{\partial\theta}\right) = 0$$

$$\dot{\varepsilon}_{r\theta} = \frac{1}{2}\left(\frac{1}{r}\frac{\partial v_r}{\partial\theta} + \frac{\partial v_\theta}{\partial r} - \frac{v_\theta}{r}\right) = \frac{v_1}{2r}\left\{\frac{3m_1(m_1^2-1)^2\sin^2 2\theta}{4\left[1+(m_1^2-1)\cos^2\theta\right]^{\frac{5}{2}}} + \frac{m_1(m_1^2-1)\cos 2\theta}{\left[1+(m_1^2-1)\cos^2\theta\right]^{\frac{3}{2}}} + \frac{m_1}{\left[1+(m_1^2-1)\cos^2\theta\right]^{\frac{1}{2}}}\right\} \tag{15}$$

For the strain rate tensor derived in Eq. (15) we get

$$\dot{\varepsilon}_{rr} + \dot{\varepsilon}_{\theta\theta} + \dot{\varepsilon}_{zz} = 0 \tag{16}$$

$$\dot{\varepsilon}_{ij}\dot{\varepsilon}_{ij} = 2\dot{\varepsilon}_{r\theta}^2 \tag{17}$$

Eq. (16) proves that the velocity field in Eq. (14) satisfies the incompressibility condition (continuity equation), therefore it is a kinematically admissible velocity field.

The first integral term in the right side of Eq. (1) would be

$$\dot{W}_{def} = 2\int_v \bar{k}\sqrt{\frac{1}{2}\dot{\varepsilon}_{ij}\dot{\varepsilon}_{ij}}dV = 2\int_{V_{PDZ}} \bar{k}\dot{\varepsilon}_{r\theta}w\cdot dl\cdot dh \tag{18}$$

where dV is the differential volume element shown in Fig. 2, w is the material thickness (normal to the paper), dl and dh are respectively the length and the height of the differential element. For a function written as

$$\vec{r} = x(\theta)\,\vec{i} + y(\theta)\,\vec{j} + z(\theta)\,\vec{k} \tag{19}$$

the differential length element can be calculated as

$$dl = \sqrt{\left(\frac{\partial x(\theta)}{\partial \theta}\right)^2 + \left(\frac{\partial y(\theta)}{\partial \theta}\right)^2 + \left(\frac{\partial z(\theta)}{\partial \theta}\right)^2}\, d\theta \tag{20}$$

Substituting Eq. (5) into Eq. (20), the differential length element in Fig. 2 is given by

$$dl = \sqrt{\frac{m_1^2 a^2 \left[(m_1^4 - 1)\cos^2\theta + 1\right]}{\left[1 + (m_1^2 - 1)\cos^2\theta\right]^3}}\, d\theta \tag{21}$$

Noting Eq. (4), Eq. (21) can also be expressed as

$$dl = \frac{\sqrt{(m_1^4 - 1)\cos^2\theta + 1}}{1 + (m_1^2 - 1)\cos^2\theta} r d\theta \tag{22}$$

The differential height element dh shown in Fig. 2 is determined as follows:

$$\text{at exit}: \theta = \frac{\pi}{2}, dh = \frac{dy}{\sin\varphi} = \sqrt{1 + \left(\frac{\lambda}{\xi} - \frac{\xi}{\lambda}\right)^2}\, dy \tag{23}$$

$$\text{at entrance}: \ \theta = 0, dh = \frac{dy}{\sin\varphi}\frac{EA}{EF} = \frac{\lambda}{\xi} dy \tag{24}$$

Here, a linear relation between the variation of dh with θ is assumed for simplicity, then

$$dh = \frac{\lambda}{\xi}\left\{1 + \frac{2\theta}{\pi}\left[\sqrt{\frac{\xi^2}{\lambda^2} + \left(1 - \frac{\xi^2}{\lambda^2}\right)^2} - 1\right]\right\} dy \tag{25}$$

Thus the differential volume element dV is given by

$$dV = w \cdot dl \cdot dh = \frac{\lambda w r}{\xi}\frac{\sqrt{(m_1^4 - 1)\cos^2\theta + 1}}{1 + (m_1^2 - 1)\cos^2\theta} \times \left\{1 + \frac{2\theta}{\pi}\left[\sqrt{\frac{\xi^2}{\lambda^2} + \left(1 - \frac{\xi^2}{\lambda^2}\right)^2} - 1\right]\right\} d\theta dy \tag{26}$$

The second integral in the right side of Eq. (1) is the power dissipated on the velocity discontinuity surfaces. As no velocity discontinuity occurs when the material enters and leaves the PDZ, the only velocity discontinuity surface is the PDZ and DMZ boundary, and the power dissipated on it is

$$\dot{W}_{Sv} = \int_{S_{DMZ}} k\, \Delta v\, dS_{DMZ} = \int_{S_{DMZ}} \bar{k}\, \Delta v\, w \cdot dl_{AF} \tag{27}$$

where dl_{AF} is the differential length element on the elliptical curve AF and can be obtained when Eq. (21) is applied on the curve with vertical axial length $2a = 2b/(\lambda/\xi) = 2\xi D_2/(\lambda/\xi) = 2\xi^2 D_2/\lambda$, where $\xi^2 D_2/\lambda$ is the height of DMZ (see Fig. 2), thus

$$dl_{AF} = \sqrt{\frac{m_1^2\left[(m_1^4 - 1)\cos^2\theta + 1\right]}{\left[1 + (m_1^2 - 1)\cos^2\theta\right]^3}}\, \frac{\xi^2 D_2}{\lambda} d\theta \tag{28}$$

The related velocity discontinuity variable is

$$\Delta v = v_{PDZ} = \sqrt{v_r^2 + v_\theta^2} \tag{29}$$

The third term in the right side of Eq. (1) is the internal power dissipated by the friction and can be broken into four parts (see Fig. 3):

Part 1 – The power dissipated on friction between the material in the region I and the die front and back walls:

$$\dot{W}_{Sf_1} = 2\int_{S_{PDZ}} m\bar{k}\, \Delta v_1\, dS_{PDZ} \tag{30}$$

where dS_{PDZ} is the same as the differential surface element used in dV for the calculation of deformation power, and Δv_1 is the same as the one used in the previous part:

$$dS_{PDZ} = dh \cdot dl = \frac{\lambda r}{\xi}\frac{\sqrt{(m_1^4 - 1)\cos^2\theta + 1}}{1 + (m_1^2 - 1)\cos^2\theta} \times \left\{1 + \frac{2\theta}{\pi}\left[\sqrt{\frac{\xi^2}{\lambda^2} + \left(1 - \frac{\xi^2}{\lambda^2}\right)^2} - 1\right]\right\} d\theta dy \tag{31}$$

$$\Delta v_1 = v_{PDZ} = \sqrt{v_r^2 + v_\theta^2} \tag{32}$$

Part 2 – The power dissipated on friction between the material in region III and the die front and back walls is

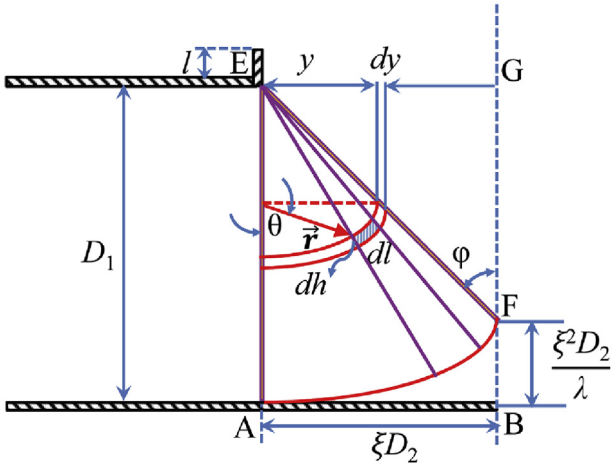

Fig. 2. Illustration of the differential volume element dV.

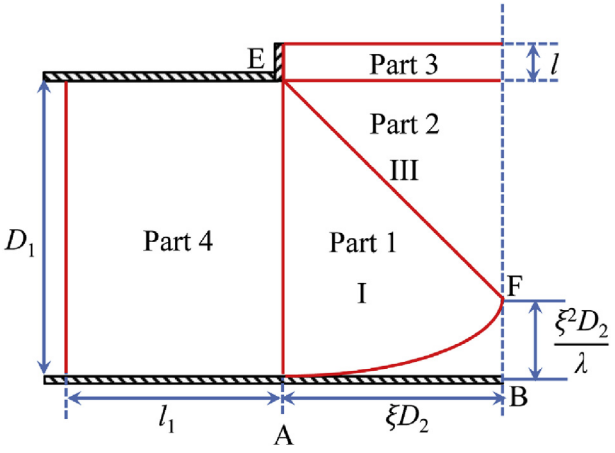

Fig. 3. Illustration of the internal power dissipated by the friction.

$$\dot{W}_{S_{f2}} = 2\int_{S_{f2}} mk_f\,\Delta v_2\,dS_{f2} = mk_f v_1 D_1^2\left(1-\frac{\xi^2}{\lambda^2}\right) \tag{33}$$

where k_f is the yield strength of the material after it has experienced plastic deformation, $\Delta v_2 = v_3 = \lambda v_1/\xi$ is the velocity discontinuity variable, S_{f2} is the related frictional surface given by

$$S_{f2} = \frac{1}{2}\xi D_2\left(D_1 - \frac{\xi^2 D_2}{\lambda}\right) = \frac{\xi}{2\lambda}D_1^2\left(1-\frac{\xi^2}{\lambda^2}\right) \tag{34}$$

Part 3 – The power dissipated on friction between the material in the die exit channel and die walls:

$$\dot{W}_{S_{f3}} = \int_{S_{f3}} mk_f\,\Delta v_3\,dS_{f3} = \lambda mk_f(2\xi D_2 + w)\frac{lv_1}{\xi} \tag{35}$$

where $\Delta v_3 = v_3 = \lambda v_1/\xi$ is the velocity discontinuity variable, $S_{f3} = (2\xi D_2 + w)l$ is the frictional surface of the exit channel, l is the exit channel (die bearing land) length.

Part 4 – The power dissipated on friction between the material in the die entrance channel (before entering region I) and die walls is

$$\dot{W}_{S_{f4}} = \int_{S_{f4}} mk_0\,\Delta v_4\,dS_{f4} = 2mk_0(D_1 + w)l_1 v_1 \tag{36}$$

where k_0 is the initial yield shear strength of the material, $\Delta v_4 = v_1$ is the velocity discontinuity which is constant, $S_{f4} = 2(D_1 + w)l_1$ is the frictional surface of the entrance channel with respect to v_1, l_1 is the transient billet length with velocity v_1 in the entrance channel.

In the DVSE process there is no external tension. So, in every instance the last term in the right side of Eq. (1) is $\int_{S_t} P_i v_i\,dS = 0$. The internal power dismissed in the other side (regions II, IV etc.) has similar characteristics and can be obtained by substituting ξ, v_1, l_1 in the above $\dot{W}_{def}$, $\dot{W}_{Sv}$, $\dot{W}_{S_f}$ with $1-\xi, v_2, l_2$, respectively. The total internal power consumed for the process $\dot{W}_i$ can be calculated by summing all the components as

$$\dot{W}_i = \dot{W}_{def} + \dot{W}_{Sv} + \dot{W}_{S_f} \tag{37}$$

For a given extrusion ratio λ and extrusion velocity ratio v_2/v_1, parameter D_1/D_2 is fixed at any extrusion time, material coefficients $(\bar{k}, k_0, k_f)$ are also constants determined by the experiment, the total power in equation above is a function of the eccentricity ratio ξ. According to the upper-bound theorem, the actual solution for ξ is obtained when $\dot{W}_i$ given in Eq. (37) reaches a minimum, i.e. differentiating the total power with respect to ξ and set the derivative equal to zero:

$$\frac{\partial \dot{W}_i}{\partial \xi} = 0 \tag{38}$$

The external supplied energy rate is

$$\dot{W}_e = \int_{S_c} P_i v_i dS = (P_1 v_1 + P_2 v_2)D_1 w \tag{39}$$

According to the upper bound theorem, the upper-bound solution is equal to or higher than the actually required force in metal forming process, i.e. the total power consumed for the process should be supplied by the upper bound of the external force, therefore we have

$$\dot{W}_{i,min} = \dot{W}_{eu} = (P_{1u}v_1 + P_{2u}v_2)D_1 w \tag{40}$$

stating that the external work done is equal to the internal energy consumed. Here, $\dot{W}_{eu}$, P_{1u} and P_{2u} are the upper bound solutions on $\dot{W}_e$, P_1 and P_2, respectively. Minimising P_{1u} and P_{2u} with respect to parameter ξ determines the best upper bound on the value of P_1 and P_2.

2.2. Determination of the extrudate curvature and effective strain

Fig. 4 illustrates the linear velocity distribution in the rectangular exit die, which is divided into two parts, namely ξD_2 and $(1-\xi)D_2$. The extrudates flowing out of these two parts per unit time can be regarded as two "prisms" determined by the axial velocity v_x, whose centres of volume (mass) are O_3 and O_4 with axial material flow velocities $v_3 = \lambda v_1/\xi, v_4 = \lambda v_2/(1-\xi)$, respectively. The y-coordinates (local x–y–z reference system) of the centres of volume (mass) of the axial velocity prisms can be given by

$$\bar{y}_3 = \frac{\int_V y dV_3}{V_3} = \frac{\int_{S_3} y v_x dS_3}{S_3 v_3}$$

$$\bar{y}_4 = \frac{\int_V y dV_4}{V_4} = \frac{\int_{S_4} y v_x dS_4}{S_4 v_4} \tag{41}$$

where V_3, V_4 are the related volumes and dS_3, dS_4 are surface elements. Using geometrical relations between parameters of Fig. 4, the curvature radius and curvature of the exit profile have been obtained using the following equations:

$$R_c = \frac{\bar{y}_4 v_3 - \bar{y}_3 v_4}{v_3 - v_4} \tag{42}$$

$$\kappa = \frac{1}{R_c} \tag{43}$$

The detailed derivation can be seen in Appendix A.

The effective strain is determined by multiplying the effective strain rate by the deformation time. The effective strain rate is

$$\bar{\dot{\varepsilon}} = \sqrt{\frac{2}{3}\dot{\varepsilon}_{ij}\dot{\varepsilon}_{ij}} = \frac{2}{\sqrt{3}}\dot{\varepsilon}_{r\theta} \tag{44}$$

where $\dot{\varepsilon}_{r\theta}$ is given in Eq. (15) and is a function of θ. Here a mean value of the effective strain rate $\bar{\dot{\varepsilon}}_m$ is used to calculate the effective strain, which is

$$\bar{\varepsilon}_m = \frac{\int_{V_{PDZ}} \bar{\dot{\varepsilon}}\,dV}{\int_{V_{PDZ}} dV} = \frac{2\int_{V_{PDZ}} \dot{\varepsilon}_{r\theta}\,dV}{\sqrt{3}\int_{V_{PDZ}} dV} \tag{45}$$

where dV is the differential volume element given in Eq. (26). The punch stroke needed for replacing the material from the PDZ with the material in the entrance channel is obtained using the volume constancy:

$$D_1 w l_1' = \int_{V_{PDZ}} dV \tag{46}$$

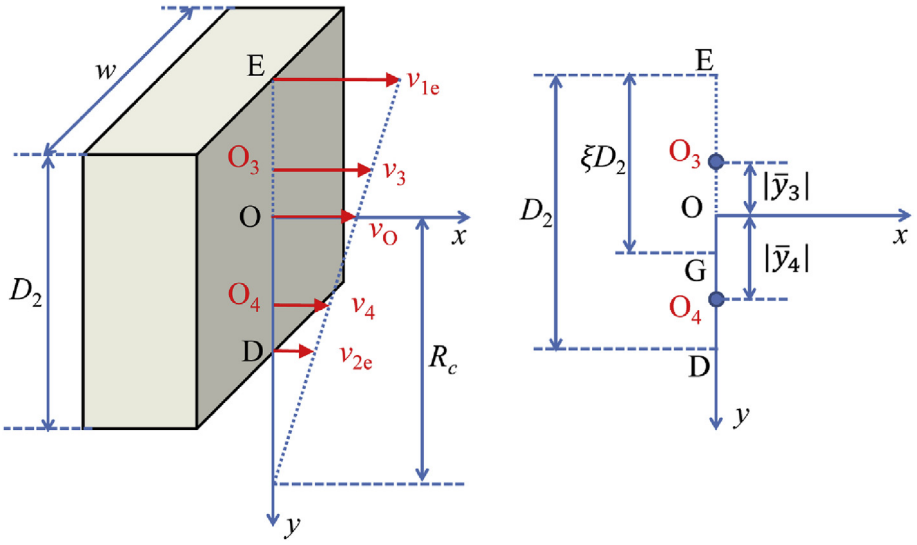

Fig. 4. The linear velocity distribution in the rectangular die exit orifice and the bending curvature.

where l_1' is the punch stroke needed. The deformation time is equal to the time taken for the punch to produce a stroke l_1':

$$t = \frac{l_1'}{v_1} \tag{47}$$

Thus the effective strain can be obtained by multiplying Eq. (45) by Eq. (47):

$$\bar{\varepsilon} = \bar{\dot{\varepsilon}}_m t \tag{48}$$

3. Experimental and finite element modelling details

The aluminium alloy AA1050 was used for tests, which was annealed at 450 °C for 1 h. Uniaxial compression tests were first conducted for a 50% reduction in height on specimens of 12 mm in height and 8 mm in diameter at room temperature (23 °C), giving an initial shear yield value of 20 MPa and a stress–strain relation as $\sigma = 145.5\varepsilon^{0.296}$, from which a final shear yield strength of 91 MPa and a mean shear flow stress of 74 MPa were obtained. The obtained true stress–strain data were also used in the material model of the finite element analysis. Finite element modelling using Deform-3D was conducted to better understand the extrusion process, $m = 0.3$ was adopted [23]. The dimension of the original billet was $D_1 = w = 25.6$ mm, the billet length was 130 mm. The parameters varied during the modelling were the width D_2 of the die exit channel, extrusion velocity v_2 of the lower punch. The velocity of the upper punch was fixed at $v_1 = 1$ mm/s, and v_2 of values 0, 0.333, 0.5, 0.667 and 1 mm/s were chosen, thus the velocity ratio v_2/v_1 of values 0, 1/3, 1/2, 2/3, and 1 were applied. D_2 of values 20 and 15 mm were studied, leading to a extrusion ratio D_1/D_2 of values 1.28 and 1.71 respectively. The extrusion tooling was assumed to be non-deformable and only the billet was deformable, the thicknesses of the punch and the extrusion container wall were simplified to be 1 mm, the bearing length was 2 mm as in practical die [23]. The billet in the FE model was meshed with tetrahedral elements. The absolute mesh density was used as the general meshing method, where the minimum size of an element was set as 0.5 mm and the size ratio was 2. A mesh window with an increased element density was applied to the billet around the die exit orifice to generate local finer elements. The element size in this mesh window was set as 0.3 mm. These mesh sizes were determined by refining them until reaching the convergence of the calculated value to judge the validity. The initial temperatures of the aluminium billet AA1050, the extrusion tooling and the ambient air temperature were 23 °C (i.e., room temperature). The process was modelled as an isothermal process, the temperature rise of the billet was considered negligible because of the limited extrusion time.

4. Results and discussion

4.1. Comparison of the flow patterns

The flow patterns of the billet (2 mm interval) are shown in Fig. 5 from the current model. The finer flow patterns (1 mm interval) of the deformation zone are also shown to reveal the dead metal zone (DMZ). A dividing line passing through the vertex of the DMZ is drawn in Fig. 5 to obtain the eccentricity ratio variable ξ and height of the DMZ. The results are illustrated respectively in Fig. 6a and b for comparison. The height of the DMZ from theoretical analysis is $\xi^2 D_2/\lambda$, as shown in Fig. 2. It can be seen from Figs. 5 and 6 that there is a good agreement between the FE modelling and the theoretical results, though some small differences exist when v_2/v_1 is close to 0. A clear DMZ is found on the edge of the billet opposite to the side where the material flows out. The two boundary lines of the DMZ come from the corresponding two extrusion punches, respectively. The height of the DMZ decreases as the velocity ratio v_2/v_1 and the extrusion ratio increase. The asymmetrical distortion of the initial flow line interval after extrusion suggests that asymmetrical material flow occurs near the die exit, due to the differential extrusion velocities of upper and lower punches.

4.2. Comparison of the extrusion pressure

Fig. 7a compares the extrusion pressure vs. stroke curves obtained from the theoretical analysis and FE modelling, at velocity ratio $v_2/v_1 = 0$ and extrusion ratios $\lambda = 1.28, 1.71$, respectively. It shows that there is a good agreement between the theoretical model and FE modelling. It is worth noting that the extrusion pressures predicted by the theoretical analysis are greater than those obtained from the FE modelling, especially at the initial stage. The difference gradually decreases as the stroke proceeds, and the maximum extrusion pressures at the stable stage of the FE

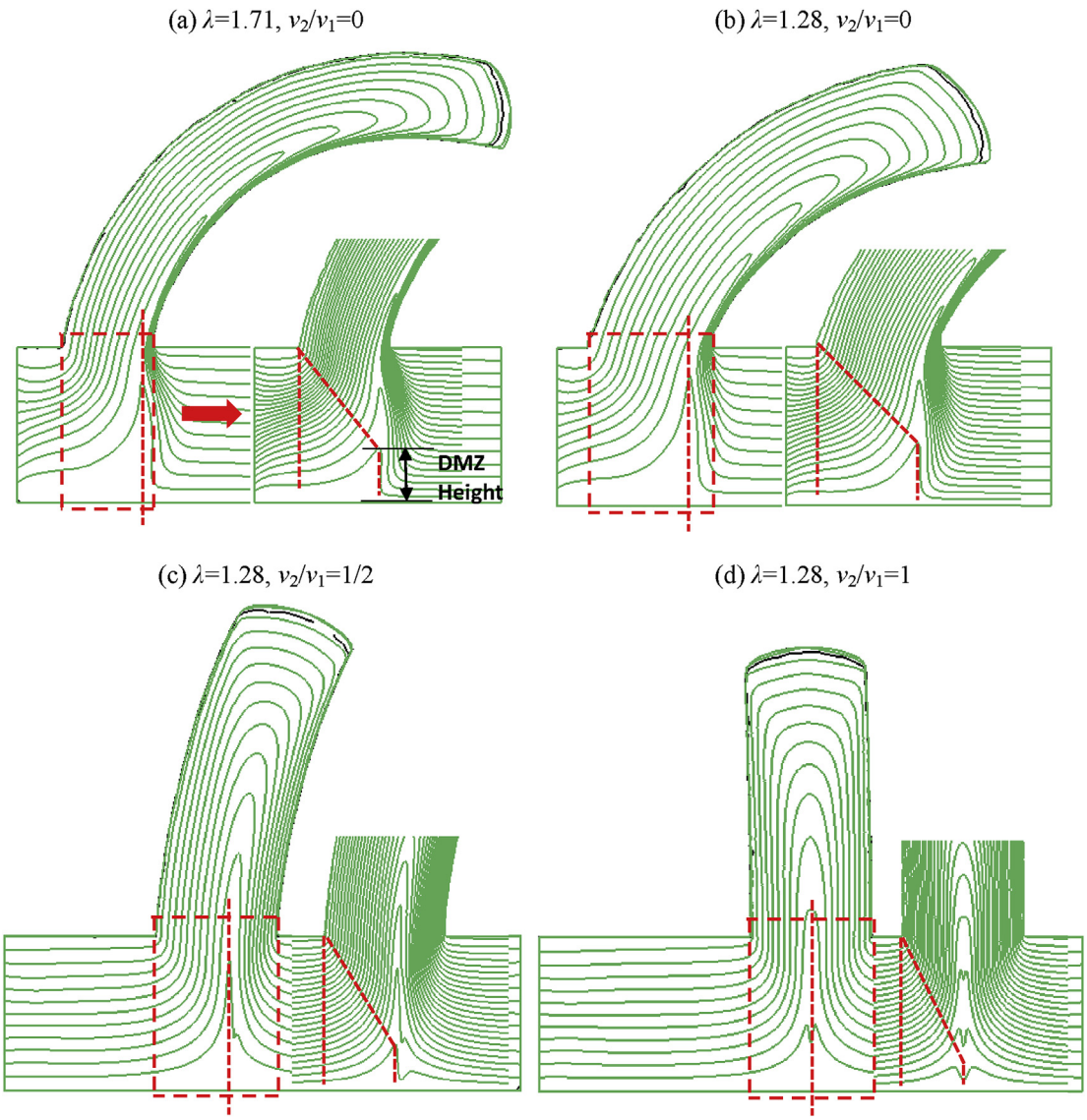

Fig. 5. Flow patterns at velocity ratios $v_2/v_1 = 0–1$ and extrusion ratios $\lambda = 1.28, 1.71$, respectively.

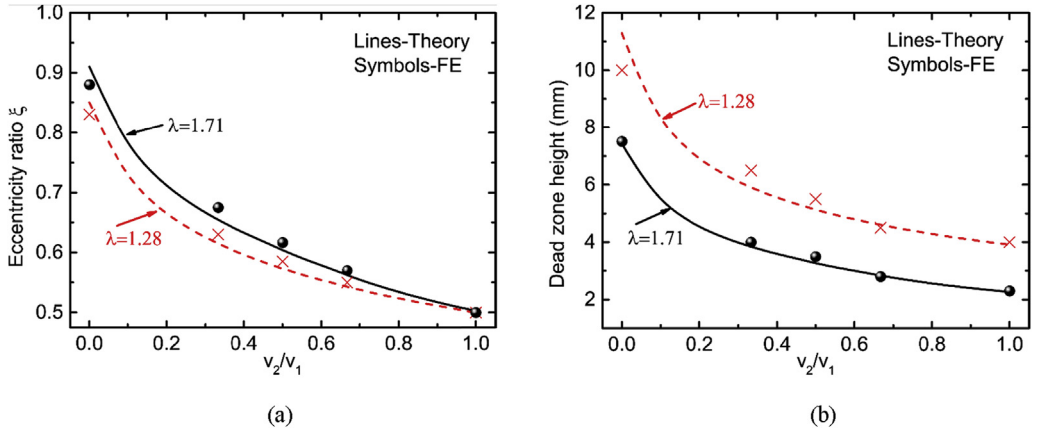

Fig. 6. Comparison of (a) eccentricity ratio ξ, (b) height of the DMZ, at velocity ratios $v_2/v_1 = 0–1$ and extrusion ratios $\lambda = 1.28, 1.71$, respectively.

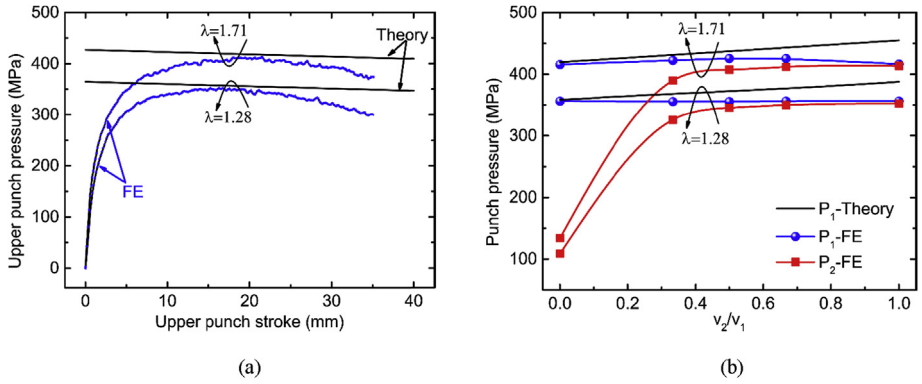

Fig. 7. Comparison of (a) extrusion pressure-stroke curves at velocity ratio $v_2/v_1 = 0$, (b) extrusion pressure vs. velocity ratios curves, with extrusion ratios $\lambda = 1.28, 1.71$, respectively.

modelling become quite close to the theoretical results. This deviation is typical of the upper bound theory. The pressure gradually decreases as the stroke proceeds further due to the decrease of frictional surface areas in the entrance channel. Fig. 7b shows the extrusion pressure vs. velocity ratio curves. The stroke used in the theoretical analysis is determined from FE modelling where the extrusion pressure P_1 of the upper punch reaches peak value. The extrusion pressure P_2 for the lower punch at this extrusion moment was also extracted. It can be seen that a reasonable agreement is achieved, though the theoretically predicted values are always slightly higher. The upper punch has a greater extrusion pressure than that of the lower punch when $v_2/v_1 < 1$, implying that the extrusion pressure P_2 for the lower punch has not reached the maximum value yet when P_1 reaches peak value. The difference in the two extrusion pressures gradually decreases as v_2 approaches v_1, which becomes negligible when $v_2 = v_1$.

4.3. Comparison of the extrudate curvature

The material flow velocity over the die exit orifice is firstly obtained from FE modelling, as shown in Fig. 8, which is then compared with that calculated from theoretical analysis in Fig. 9a. The extrudate curvature is compared in Fig. 9b. The values of the curvatures from FE modelling are estimated by fitting the result images with best-fit circles with the same scale. After getting the radius R_c of the circle, the curvature is calculated as $1/R_c$. Fig. 9a and b show that there is a good agreement on the predicted velocity and curvature, although the theoretically predicted curvature is slightly greater than that of the FE modelling especially when v_2/v_1 is small. This may be due to the fact that the material flowing out of the die exit orifice is assumed to be two independent parts controlled by the two extrusion punches separately, but in reality the velocity of these two parts are mutually constrained, the faster upper part may

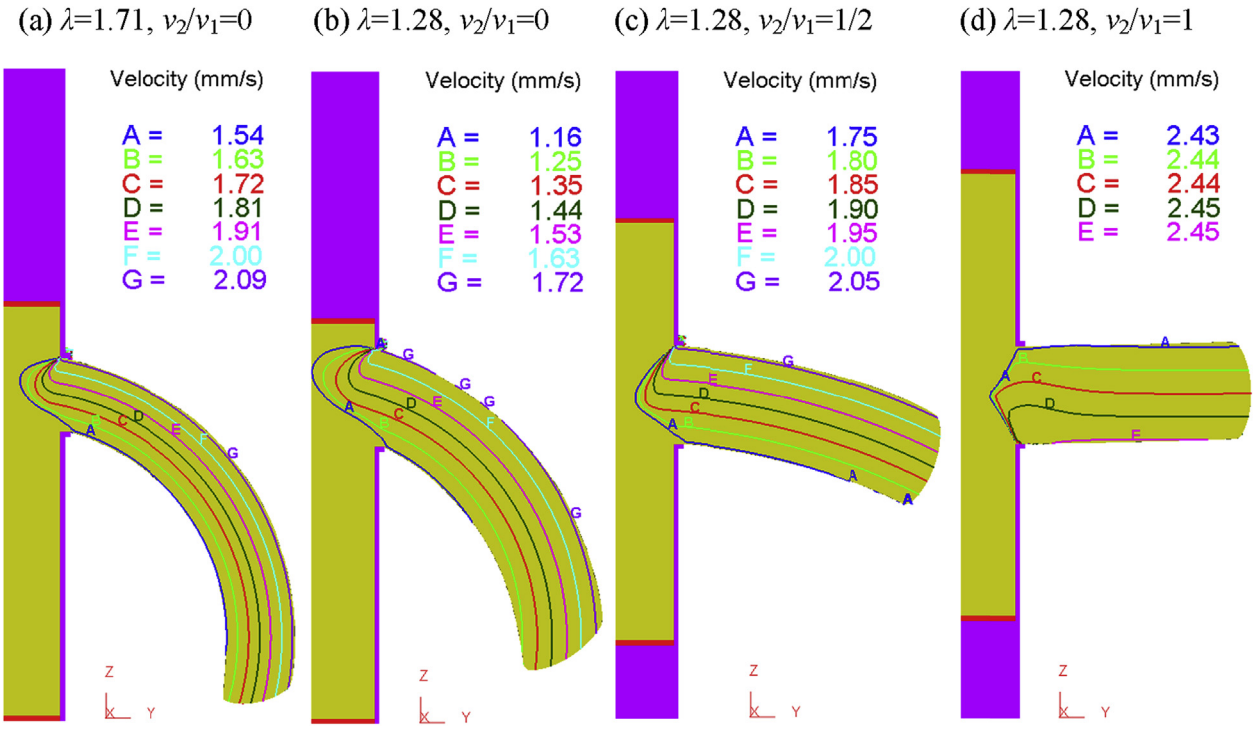

Fig. 8. Simulated material flow velocity distribution across the die exit orifice, at velocity ratios $v_2/v_1 = 0–1$ and extrusion ratios $\lambda = 1.28, 1.71$, respectively.

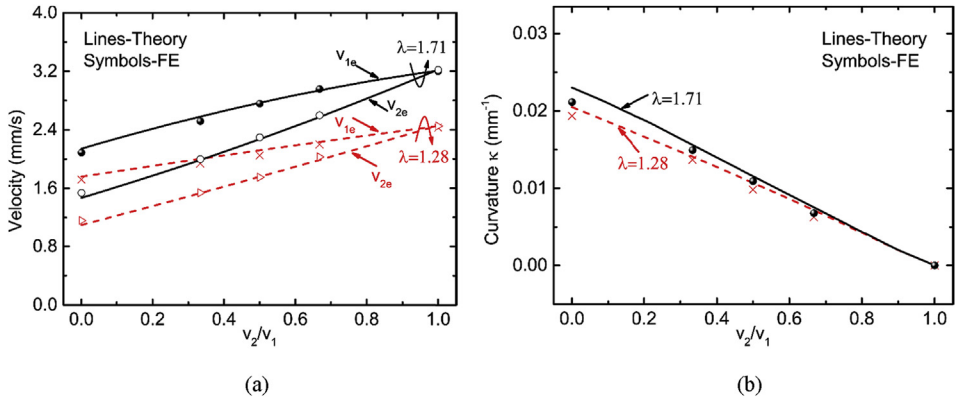

Fig. 9. Comparison of (a) material flow velocities across the die exit orifice, (b) extrudate curvature, at velocity ratios $v_2/v_1 = 0$–1 and extrusion ratios $\lambda = 1.28, 1.71$, respectively.

have a "pull" effect on the slower lower part, which in turn may have a "drag" effect on the faster upper part. Another reason might be that the effect of friction at the bearing land on the die exit velocity and thus the profile curvature is not considered due to the short bearing length (2 mm). However it could still have an 'unbending' or straightening effect on the extrudate, which needs further investigation. All these factors make the predicted v_{1e} greater and v_{2e} smaller than that of FE modelling, especially when the velocity difference of the two extrusion punches is greater, i.e. v_2/v_1 is smaller, as can be seen in Fig. 9a. The difference of the predicted velocity between the theoretical analysis and FE modelling gradually decreases as the extrusion ratio λ decreases and the velocity ratio v_2/v_1 increases towards 1, which is in accordance with and explains the curvature difference shown in Fig. 9b. It can also be seen from Fig. 9b that the curvature obtained from the FE modelling is less sensitive to the extrusion ratio than that obtained from the analytical model, which is in accordance with previous work on curved round bars using the simple shear model and FE modelling [29].

4.4. Comparison of the effective strain

As discussed before the original extrusion die orifice can be divided into two exit channels and the DVSE process can be reasonably regarded as two equal or non-equal channel angular extrusion (ECAE or NECAE) processes depending on the eccentricity ratio ξ. For a NECAE die without rounding of the corners at the intersection of the channels, the simple shear model which assumes the material experiences an abrupt shearing gives the value of shear strain in one pass as [31].

$$\gamma = \cot \alpha_1 + \cot \alpha_2 \tag{49}$$

where α_1 and α_2 are the angles of the intersection plane with the entry and exit channels, respectively. For a 90° NECAE die, the value of effective strain can be calculated from Eq. (49) as

$$\bar{\varepsilon} = \gamma \Big/ \sqrt{3} = (D_i/D_e + D_e/D_i) \Big/ \sqrt{3} \tag{50}$$

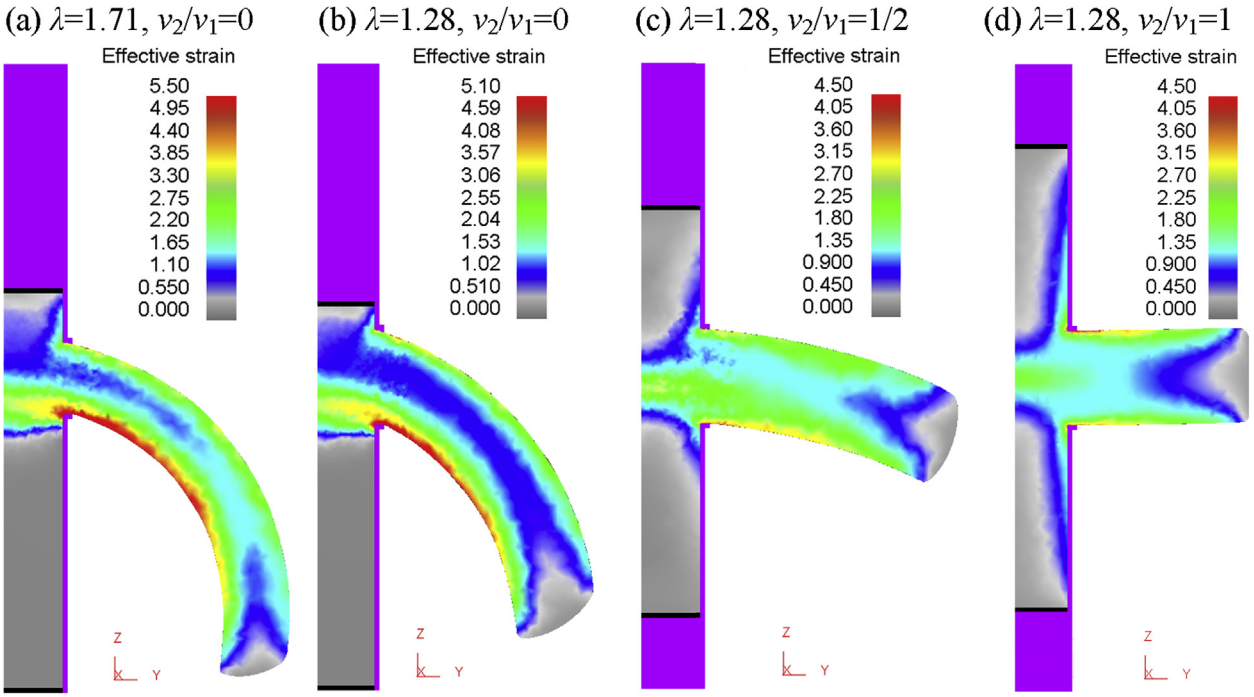

Fig. 10. Effective strain contours at velocity ratios $v_2/v_1 = 0$–1 and extrusion ratios $\lambda = 1.28, 1.71$, respectively.

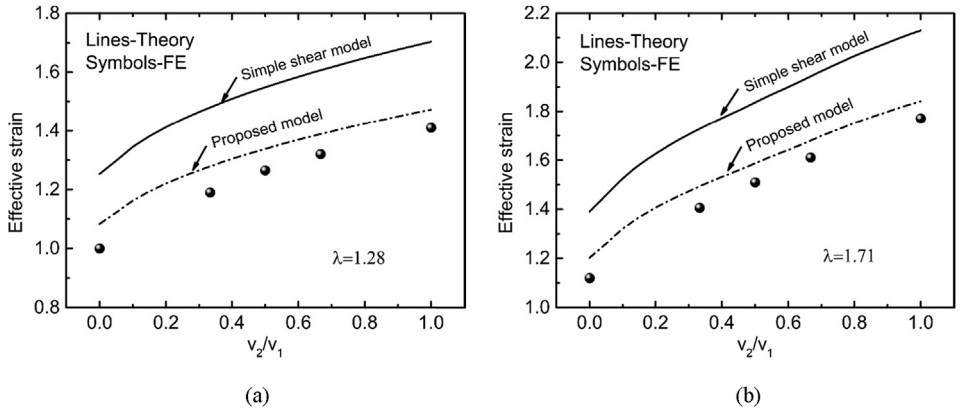

Fig. 11. Comparison of the effective strain of the extrudate: (a) $\lambda = 1.28$, (b) $\lambda = 1.71$.

where D_i and D_e are widths of the entry channel and the exit channel, respectively. Here, $D_i = D_1 = 25.6$ mm is the same for all velocity ratios and extrusion ratios. Only the effective strain of outside bending part of the profile is calculated here, thus $D_e = \xi D_2$, where ξ is shown in Fig. 6a.

Fig. 10 shows the effective strain of the profile obtained from FE modelling. It can be seen that severe plastic deformation (SPD) occurs in the DVSE process, although certain inhomogeneous deformation in local regions exists. The inside bending region of the profile has the maximum localised deformation, which decreases as the extrudate curvature decreases, namely as the extrusion ratio decreases and the velocity ratio v_2/v_1 increases. Here, the mean value of the effective strain over the cross-section of the outside bending part of the profile at the die orifice is extracted from FE modelling and shown in Fig. 11. The effective strain obtained from the simple shear model and the proposed flow field model is also given for comparison. Fig. 11 shows that the effective strain obtained from the simple shear model is greater than those from the proposed flow field model and the FE model, where the latter two are very close. This implies that by distributing the plastic deformation zone (PDZ) over a region instead of an abrupt and concentrated shearing deformation on a single line, the predicted effective strain will decrease, which is more close to the realistic effective strain. This result is in accordance with other studies done on ECAE [32], where the effective strain in one pass is obtained as a function of the n exponent of the continuous flow line function and increases with n, and the simple shear case $(n \to \infty)$ gives the upper limit value $2/\sqrt{3} = 1.15$ of the effective strain.

5. Conclusions

A continuous fan-shaped flow line model is developed based on the upper bound theorem to better analyse the deformation field of a novel extrusion process, differential velocity sideways extrusion (DVSE), previously proposed by the authors for forming curved profiles. The predicted flow patterns, extrusion pressure, extrudate curvature, and effective strain by the analytical model agree well with the FE modelling results. It was concluded that the height of the dead metal zone (DMZ) decreases as the velocity ratio v_2/v_1 and the extrusion ratio increase. A lower extrusion pressure is needed for a punch with a lower velocity, which increases with the increase of its velocity. Bending curvatures of the extruded profiles can be actively controlled in the DVSE process, which decrease as the extrusion velocity ratio v_2/v_1 increases and the extrusion ratio decreases. Severe plastic deformation (SPD) occurs in the DVSE process in a way similar to the equal channel angular extrusion (ECAE), but with a greater effective strain level than that per pass in ECAE. The new fan-shaped flow line model predicts a smaller but more realistic effective strain than the discontinuous shear approach.

Acknowledgement

The financial support from the President's PhD Scholarship of Imperial College London is greatly appreciated.

Appendix A. Determination of the extrudate curvature

Fig. 4 shows the linear velocity distribution in a rectangular zone. In this figure, D_2 is the width of the extrudate and v_3 and v_4 are the axial velocities at coordinates $\bar{y}_3$ and $\bar{y}_4$, respectively. R_c is the radius of the exit profile curvature. Assume after a finite time element Δt, the extrudates at points O_3, O_4 move Δd_3 and Δd_4, due to $\Delta d_3 > \Delta d_4$ the exit profile will not come out straight and will have a bending angle $\Delta\theta_c$, the following kinematic relations exist:

$$\Delta d_3 = v_3 \Delta t \tag{A1}$$

$$\Delta d_4 = v_4 \Delta t \tag{A2}$$

The related geometrical relations are

$$\Delta d_3 = \Delta\theta_c (R_c - \bar{y}_3) \tag{A3}$$

$$\Delta d_4 = \Delta\theta_c (R_c - \bar{y}_4) \tag{A4}$$

Substituting Eqs. (A3)–(A4) into Eqs. (A1)–(A2), the curvature radius of the exit profile is given by

$$R_c = \frac{\bar{y}_4 v_3 - \bar{y}_3 v_4}{v_3 - v_4} \tag{A5}$$

According to the law of conservation of mass:

$$v_o = \frac{D_1}{D_2}(v_1 + v_2) = \lambda(v_1 + v_2) \tag{A6}$$

v_x can be expressed as a function of $\bar{y}_3$ as

$$v_x = \frac{v_3 - v_o}{\bar{y}_3} y + v_o \tag{A7}$$

Substituting Eqs. (A6)–(A7) into Eq. (41), $\bar{y}_3$ is implicitly given by

$$\bar{y}_3 = \frac{\int_{S_3} y v_x dS_3}{S_3 v_3} = \frac{\int_{-\frac{D_2}{2}}^{(\xi-\frac{1}{2})D_2} y\left(\frac{v_3 - v_o}{\bar{y}_3} y + v_o\right) w dy}{\xi D_2 w v_3}$$
$$= \frac{(v_3 - v_o)D_2^2}{3\bar{y}_3 \xi v_3}\left[\frac{1}{8} + \left(\xi - \frac{1}{2}\right)^3\right] - \frac{v_o D_2}{2\xi v_3}\left[\frac{1}{4} - \left(\xi - \frac{1}{2}\right)^2\right] \quad (A8)$$

Thus $\bar{y}_3$ can be obtained by numerically solving the following equation:

$$\bar{y}_3^2 + g_1(\xi)\bar{y}_3 - g_2(\xi) = 0 \quad (A9)$$

where $\bar{y}_3 < 0$ should be the negative root, $g_1(\xi), g_2(\xi)$ are only functions of ξ which are expressed as

$$g_1(\xi) = \frac{v_o D_2}{2\xi v_3}\left[\frac{1}{4} - \left(\xi - \frac{1}{2}\right)^2\right] \quad (A10)$$

$$g_2(\xi) = \frac{(v_3 - v_o)D_2^2}{3\xi v_3}\left[\frac{1}{8} + \left(\xi - \frac{1}{2}\right)^3\right] \quad (A11)$$

$\bar{y}_4$ can be obtained similarly. Then v_{2e} and v_{1e} can be given by substituting $y = \pm 0.5 D_2$ respectively into Eq. (A7).

References

[1] M. Kleiner, S. Chatti, A. Klaus, Metal forming techniques for lightweight construction, J. Mater. Process. Technol. 177 (2006) 2–7.
[2] M. Schneider, G. Koehler, D. Becker, A. Selvaggio, A.E. Tekkaya, C. Munzinger, V. Schulze, M. Kleiner, Towards the flexible and near-net-shape production of three dimensionally curved extrusion profiles, Prod. Eng. Res. Dev. 4 (2010) 561–569.
[3] M. Hermes, D. Staupendahl, C. Becker, A.E. Tekkaya, Innovative machine concepts for 3D bending of tubes and profiles, Key Eng. Mater. 473 (2011) 37–42.
[4] A.E. Tekkaya, N.B. Khalifa, G. Grzancic, R. Hölker, Forming of lightweight metal components: need for new technologies, Procedia Eng. 81 (2014) 28–37.
[5] F. Paulsen, T. Welo, Cross-sectional deformations of square hollow sections in bending: part II-analytical models, Int. J. Mech. Sci. 43 (2001) 131–152.
[6] A.H. Clausen, O.S. Hopperstad, M. Langseth, Sensitivity of model parameters in stretch bending of aluminum extrusions, Int. J. Mech. Sci. 43 (2001) 427–453.
[7] J.E. Miller, S. Kyriakides, A.H. Bastard, On bend-stretch forming of aluminum extruded tubes-I: experiments, Int. J. Mech. Sci. 43 (2001) 1283–1317.
[8] J.E. Miller, S. Kyriakides, A.H. Bastard, On bend-stretch forming of aluminum extruded tubes-II: analysis, Int. J. Mech. Sci. 43 (2001) 1319–1338.
[9] J. Zhao, R.X. Zhai, Z.P. Qian, R. Ma, A study on springback of profile plane stretch-bending in the loading method of pretension and moment, Int. J. Mech. Sci. 75 (2013) 45–54.
[10] J. Liao, X. Xue, M.G. Lee, F. Barlat, J. Gracio, On twist springback prediction of asymmetric tube in rotary draw bending with different constitutive models, Int. J. Mech. Sci. 89 (2014) 311–322.
[11] Ev. Finckenstein, G. Ludowig, G. Zicke, G. Stutte, Developments in NC-sheet metal bending, especially in NC-roll bending, CIRP Ann. Manuf. Technol. 30 (1981) 163–166.
[12] S. Chatti, M. Hermes, M. Kleiner, Three-dimensional bending of profiles by stress superposition, in: D. Banabic (Ed.), Advanced Methods in Material Forming, Springer Verlag, Berlin, 2007, pp. 101–118.
[13] M. Hermes, S. Chatti, A. Weinrich, A.E. Tekkaya, Three-dimensional bending of profiles with stress superposition, Int. J. Mater. Form. 1 (2008) 133–136.
[14] S. Chatti, M. Hermes, A.E. Tekkaya, M. Kleiner, The new TSS bending process: 3D bending of profiles with arbitrary cross-sections, CIRP Ann. Manuf. Technol. 59 (2010) 315–318.
[15] M. Hermes, M. Kleiner, Method and device for profile bending, in: European Patent EP2144720B1, 2008.
[16] A. Selvaggio, D. Becker, A. Klaus, D. Arendes, M. Kleiner, Curved profile extrusion, in: A.E. Tekkaya, W. Homberg, A. Brosius (Eds.), 60 Excellent Inventions in Metal Forming, Springer Verlag, Berlin, 2015, pp. 287–292.
[17] K.B. Müller, Bending of extruded profiles during extrusion process, Mater. Forum 28 (2004) 264–269.
[18] K.B. Müller, Bending of extruded profiles during extrusion process, Int. J. Mach. Tool Manufact. 46 (2006) 1238–1242.
[19] M. Shiraishi, M. Nikawa, Y. Goto, An investigation of the curvature of bars and tubes extruded through inclined dies, Int. J. Mach. Tool Manufact. 43 (2003) 1571–1578.
[20] M. Nikawa, M. Shiraishi, Y. Miyajima, H. Horibe, Y. Goto, Production of shaped tubes with various curvatures using extrusion process through inclined die aperture, J. Jpn. Soc. Technol. Plast. 43 (2002) 654–656.
[21] Y. Takahashi, S. Kihara, K. Yamaji, M. Shiraishi, Effects of die dimensions for curvature extrusion of curved rectangular bars, Mater. Trans. 56 (2015) 844–849.
[22] W.B. Zhou, J. Lin, T.A. Dean, L.L. Wang, A novel application of sideways extrusion to produce curved aluminium profiles: feasibility study, Procedia Eng. 207 (2017) 2304–2309.
[23] W.B. Zhou, J. Lin, T.A. Dean, L.L. Wang, Feasibility studies of a novel extrusion process for curved profiles: experimentation and modelling, Int. J. Mach. Tool Manufact. 126 (2018) 27–43.
[24] K.F. Celik, N.R. Chitkara, Application of an upper bound method to off-centric extrusion of square sections, analysis and experiments, Int. J. Mech. Sci. 42 (2000) 321–345.
[25] J.S. Ajiboye, M.B. Adeyemi, Upper bound analysis for extrusion at various die land lengths and shaped profiles, Int. J. Mech. Sci. 49 (2007) 335–351.
[26] M. Rastegar, A. Assempour, A. Ghazanfari, Determination of Geometrical Parameters of the Dead Metal Zone and Exit Curvature Profile in the Extrusion Process of Non-symmetrical Flat Dies, 2012. SAE Technical Paper No. 2012-01-0052.
[27] A. Parvizi, K. Abrinia, A two dimensional upper bound analysis of the ring rolling process with experimental and FEM verifications, Int. J. Mech. Sci. 79 (2014) 176–181.
[28] Y.J. Wu, X.H. Dong, Q. Yu, Upper bound analysis of axial metal flow inhomogeneity in radial forging process, Int. J. Mech. Sci. 93 (2015) 102–110.
[29] W.B. Zhou, J.G. Lin, T.A. Dean, L.L. Wang, Analysis and modelling of a novel process for extruding curved metal alloy profiles, Int. J. Mech. Sci. 138–139 (2018) 524–536.
[30] C.T. Kwan, Y.C. Hsu, An analysis of pseudo equal-cross-section lateral extrusion through a curved channel, J. Mater. Process. Technol. 122 (2002) 260–265.
[31] D.N. Lee, An upper-bound solution of channel angular deformation, Scripta Mater. 43 (2000) 115–118.
[32] L.S. Tóth, R.A. Massion, L. Germain, S.C. Baik, S. Suwas, Analysis of texture evolution in equal channel angular extrusion of copper using a new flow field, Acta Mater. 52 (2004) 1885–1898.